SILVER PHOSPHATE NANOPARTICLE-EMBEDDED ZINC OXIDE NANOWIRE ARRAYS FOR PHOTOELECTROCHEMICAL SOLAR WATER SPLITTING

by

Pattarapa Boon-im

B.E., Chulalongkorn University, 2009

Submitted to the Graduate Faculty of

Swanson School of Engineering in partial fulfillment

of the requirements for the degree of

Master of Science in Chemical Engineering

University of Pittsburgh

2012

UNIVERSITY OF PITTSBURGH

SWANSON SCHOOL OF ENGINEERING

This thesis was presented

by

Pattarapa Boon-im

It was defended on

November 19, 2012

and approved by

Götz Veser, PhD, Professor
Department of Chemical and Petroleum Engineering

Prashant N. Kumta, PhD, Professor
Department of Chemical and Petroleum Engineering

Di Gao, PhD, Associate Professor,
Department of Chemical and Petroleum Engineering
Thesis Advisor

SILVER PHOSPHATE NANOPARTICLE-EMBEDDED ZINC OXIDE NANOWIRE ARRAYS FOR PHOTOELECTROCHEMICAL SOLAR WATER SPLITTING

Pattarapa Boon-im, M.S.

University of Pittsburgh, 2012

Conversion of solar energy to storable chemical energy has received considerable interest in the past decade due to the limited availability of fossil fuels and concerns on environmental sustainability. One of the important processes involved in producing alternative fuels by utilizing solar energy is solar water splitting. One of the challenges in solar water splitting is to identify a semiconductor material that is capable to absorb major portion of the solar spectrum and possesses proper band edge potentials to simultaneously oxidize and reduce water. An alternative approach to the direct solar water splitting is photoelectrochemical solar water splitting, which physically separates the photoanode from photocathode for water oxidation and reduction, respectively, allowing each electrode to be independently optimized.

In this work, a composite photoanode consisting of Ag_3PO_4 nanoparticles embedded into ZnO nanowire arrays is fabricated for photoelectrochemical solar water splitting. The composite photoanode takes advantage of both the high photocatalytic activity of Ag_3PO_4 nanoparticles and the fast electron transport enabled by single crystalline ZnO nanowires. Ag_3PO_4 nanoparticles are able to harness visible light and possess higher photoactivity than most known

semiconductors including $BiVO_4$ and WO_3 under visible light irradiation, thanks to the band structure of Ag_3PO_4 and the high internal surface area of Ag_3PO_4 nanoparticles. However, the efficiency of the photoanode made of Ag_3PO_4 nanoparticle films is limited by the slow electron transport between the disorderly packed Ag_3PO_4 nanoparticles and only very thin films of Ag_3PO_4 nanoparticles may be used. We have found that embedding the Ag_3PO_4 nanoparticles into ordered ZnO nanowire arrays may allow much thicker films of Ag_3PO_4 nanoparticles to be used and the photocurrent may be improved by up to six times compared to planar Ag_3PO_4/ZnO films, primarily due to the improved charge transportation enabled by the vertically ordered single crystalline ZnO nanowire arrays. Our result indicates that Ag_3PO_4 nanoparticles-embedded ZnO nanowire array is a promising composite photoanode for solar water splitting.

TABLES OF CONTENTS

LIST OF FIGURES

ACKNOWLEDGEMENT

I am sincerely thankful to my advisor, Dr. Di Gao for his continuous support and guidance throughout my study and research. This thesis would not happen to be possible without his patience, enthusiasm and extensive knowledge and experience in the field.

Besides my advisor, I am truly grateful for the insightful suggestions and advices from my thesis committees, Dr. Götz Veser and Dr. Prashant Kumta.

I would like to thank Department of Chemical and Petroleum Engineering at the University of Pittsburgh for providing the solid background in chemical engineering and the laboratory and office facilities for the completion of the thesis.

It is an honor for me to show my gratitude to my group members: Dr. Chengkun Xu, Jiamin Wu, Umang Desani, Jason Lee and Guangyu Lv for their support in a number of ways. In particular, I owe the earnest thankfulness to Dr. Chengkun Xu and Jiamin Wu for their tremendous help and knowledgeable advices.

I am obliged to all of my friends who always stood by me. I am greatly appreciated the wonderful support of the Thai Student Association of Pittsburgh especially my roommates, Wantanee Viriyasitavat and Ratiporn Munprom. Many thanks to Sasimaka Burusphat who has always served by me and dealt with my tempers, and Gun Kositchaiwat for his willingness to help and his sense of humor. It is with immense gratitude that I acknowledge the blessings from

my close friends, Savika Varaporn, Prapasri Kingklao, Titiya Sonthikaew and Pimrapat Thanusutiyaporn. I would also like to offer my regards to everyone who helped me in any respect during the completion of the thesis successfully.

Lastly, this thesis would have remained a dream had it not been for the continuous support and encouragement from my family who has been giving the endless love throughout my life. I would like to dedicate this thesis to my parents who have presented me the opportunity to study in the top ranked university and always believed in me.

1.0 INTRODUCTION

The depletion of fossil fuels and environmental sustainability has raised global concern in the twentieth century. Much research effort has been devoted to solving the challenge on how to harvest the energy from sunlight and store in chemical bonds as nature does in photosynthesis. One of the attractive approaches towards less reliance on fossil fuels is photoelectrolysis of water or solar water splitting, which generates hydrogen and oxygen from water at the semiconductor/electrolyte interface by utilizing solar energy. Solar water splitting is a truly clean process. Both of the inputs, water and sunlight, are inexpensive and abundant and the combustion of hydrogen does not produce greenhouse gases.

The water splitting reaction involves two redox half reactions which are water oxidation (or oxygen evolution) and water reduction (or hydrogen evolution) as the following: [1]

$2H_2O \rightarrow O_2 + 4H^+ + 4e^-$ $\quad E^0 (O_2/H_2O) = 1.23$ V versus NHE (1.1)

$4H^+ + 4e^- \rightarrow 2H_2$ $\quad E^0 (H^+/H_2) = 0$ V versus NHE (1.2)

The potential difference between water oxidation and reduction is 1.23 eV. Therefore, the theoretical minimum band gap of a semiconductor required for inducing water splitting is 1.23 eV. From the relationship between band gap energy and wavelength (λ) of incident light:

$$\text{Band gap (eV)} = 1{,}242/\lambda \text{ (nm)} \quad (1.3)$$

The potential difference for water splitting is equivalent to the radiation energy of a photon with a wavelength of approximately 1,000 nm. [1] [2]

1.1 PROCESSES IN PHOTOCATALYTIC WATER SPLITTING

Photocatalytic water splitting process starts from the photon absorption that creates the photogenerated electron-hole pairs (Figure 1). When a semiconductor material is radiated with photons that have equal or higher energy than the band gap energy, the photon energy is transferred to electrons. Electrons are then promoted into the conduction band where they are free to move around within the semiconductor, leaving holes in the valence band. However, such photogenerated electrons and holes are not stable and may recombine; once they recombine, the electron-hole pair is lost and the water splitting process cannot take place.

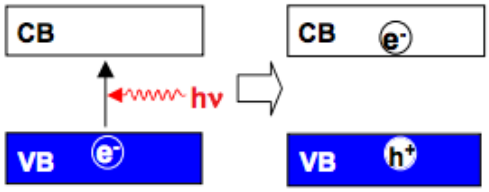

Figure 1. Electron-hole pair generated by photon absorption. [3]

The photogenerated charge carriers then migrate to the semiconductor-liquid interface where the redox reactions take place. The adsorbed water molecules on the semiconductor surface are reduced by electrons to form hydrogen and oxidized by holes to form oxygen. The overall reaction is:

$$2H_2O \rightarrow 2H_2 + O_2 \qquad (1.4)$$

The process of semiconductor-based solar water splitting is shown in Figure 2.

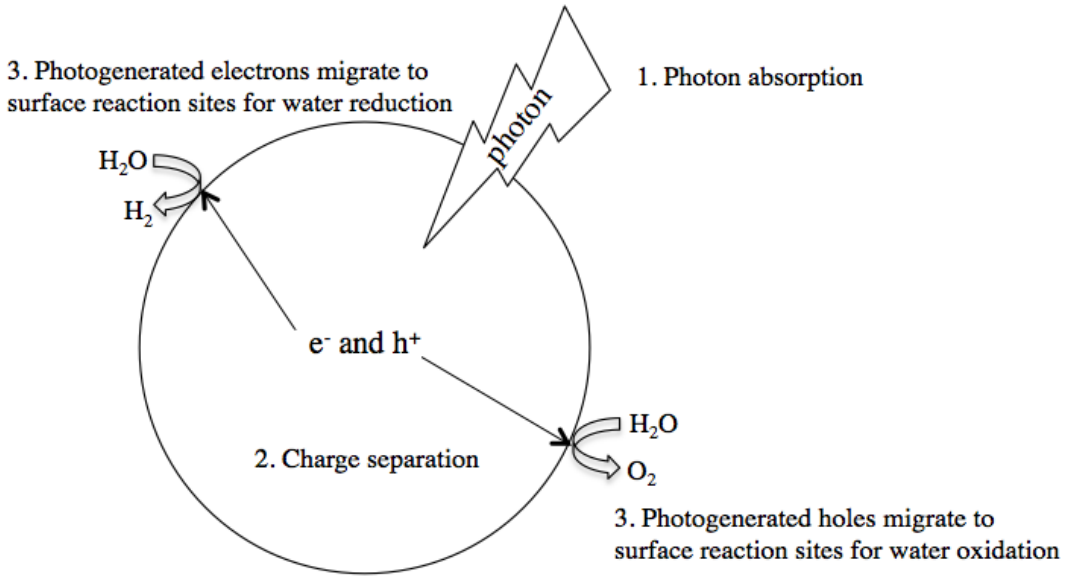

Figure 2. Schematic of photocatalytic water splitting process.

The important factors in semiconductor-based solar water splitting are the width of the energy band gap and the energy levels of the conduction band and valence band of a semiconductor material. Figure 3 represents the suitable conduction and valence bands of a semiconductor with respect to redox potential of hydrogen and oxygen for water splitting. The appropriate semiconductor for water splitting should have the bottom of the conduction band lie at more negative levels than the redox potential of water reduction and the top of valence band lie at more positive value than the redox potential of water oxidation. Furthermore, the semiconductor material should absorb a large portion of solar spectrum. Figure 4 shows the solar energy distribution, which indicates that the visible irradiation accounts for 47% of the total solar spectrum. Thus, semiconductor materials with a narrow band gap energy, less than 3 eV, may absorb a broad range of solar spectrum including visible and UV region while the semiconductor with band gaps than 3 eV wider can only absorb UV light.

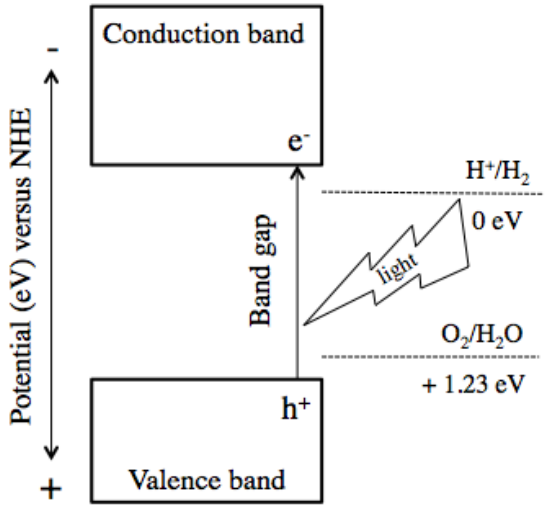

Figure 3. Solar water splitting on a semiconductor material.

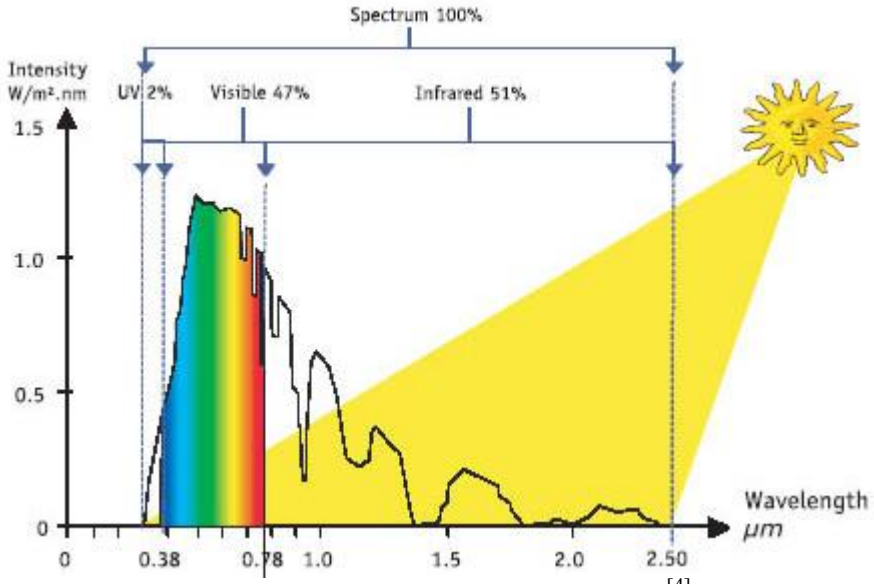

Figure 4. Solar energy distribution. [4]

The semiconductor-based photoelectrochemical solar water splitting has drawn considerable attention due to the potential to split water into usable hydrogen by harnessing the solar energy. [3] [6] [7] The energy obtained from solar utilization is very attractive because the

solar energy is an inexpensive abundant natural resource and the amount reaching the earth is gigantic. The total amount of solar energy striking the earth's surface per year is approximately 3×10^{24} J (Figure 5). [3] [5]

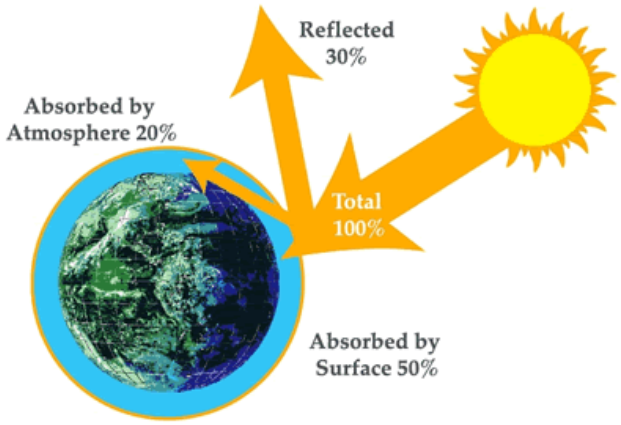

Figure 5. Solar energy to the earth. [5]

1.2 DIRECT PHOTOCATALYTIC WATER SPLITTING

Many semiconductors have been studied and fabricated during the past decades, including silicon (Si), cadmium telluride (CdTe), gallium arsenide (GaAs), titanium dioxide (TiO_2) and zinc oxide (ZnO). Despite the various research and study, the search for a single semiconductor material that can perform overall solar water splitting or direct photoelectrolysis remains challenging. Semiconductor materials that are stable under photoelectrolysis conditions, have an appropriate band structure that can simultaneously perform water reduction and oxidation and are able to absorb a significant amount of solar spectrum, have been rarely identified. Studies frequently reported that one requirement is met at the expense of another. [1] [2] [11] The semiconductor materials with narrower energy band gaps, which can absorb wider range of solar

spectrum, tend to have higher conversion efficiency. However, many studies show that these semiconductors with a narrow band gap are not suitable for long-term usage in water splitting because these materials may dissolve in aqueous solutions and the photogenerated charge carriers may react and corrode them.

1.3 PHOTOELECTROCHEMICAL SOLAR WATER SPLITTING

As an alternative approach to direct photoelectrolysis, photoelectrochemical cells physically separate the two redox half reactions so that they take place at two separated electrodes: water oxidation occurs at the anode, and water reduction occurs at the cathode. In other words, the two half-reactions, for oxygen and hydrogen evolution, respectively, occur at two different electrodes. This provides the opportunity to optimize each electrode independently since the suitable material for water oxidation might not be suitable for water reduction, and vice versa. A bias potential is usually employed to overcome the potential difference between the energy band of a semiconductor and the redox potential of water and to transfer the photogenerated electrons to a metal cathode. The relationship in band structure of various semiconductor photocatalysts and redox potential of water splitting is demonstrated in Figure 6. [2] The semiconductor material whose valence band potential is not positive enough for the water oxidation or whose conduction band potential is not negative enough for the water reduction can lead to slow or negligible water splitting. [3] By applying the bias voltage, the overpotentials required to drive water oxidation and reduction are fulfilled. Therefore, photoelectrochemical cell configuration offers more material choices for water splitting than the direct photoelectrolysis.

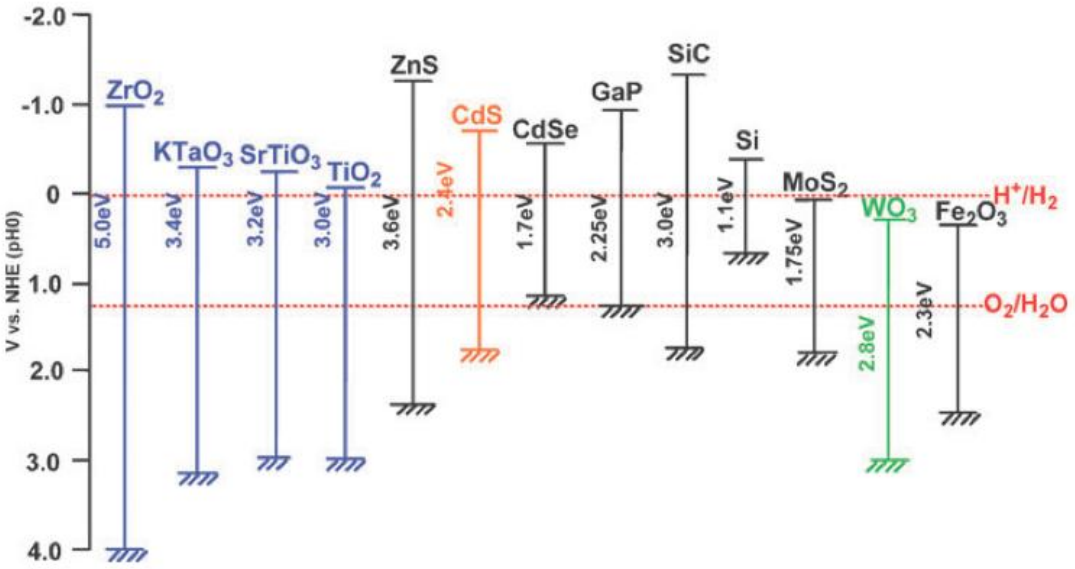

Figure 6. Relationship between band structure of various semiconductor photocatalysts and redox potential of water splitting. [2]

The photoelectrochemical solar water splitting cell was first introduced in 1972 by Honda and Fujishima. They reported water splitting using TiO_2 electrode as a photoanode and Pt as a cathode. TiO_2 is the first semiconductor material employed as a photoanode in photoelectrochemical solar water splitting cell because TiO_2 is cheap and stable over a broad range of pH. [30] Figure 7 presents the electrons and holes in TiO_2 generated upon the UV light irradiation with a wavelength less than 415 nm in Honda and Fujishima photoelectrochemical cell. The photogenerated holes oxidize water into oxygen at TiO_2 photoanode while the photogenerated electrons reduce water into hydrogen at Pt counter electrode. [1] [2] [3] [8] [9]

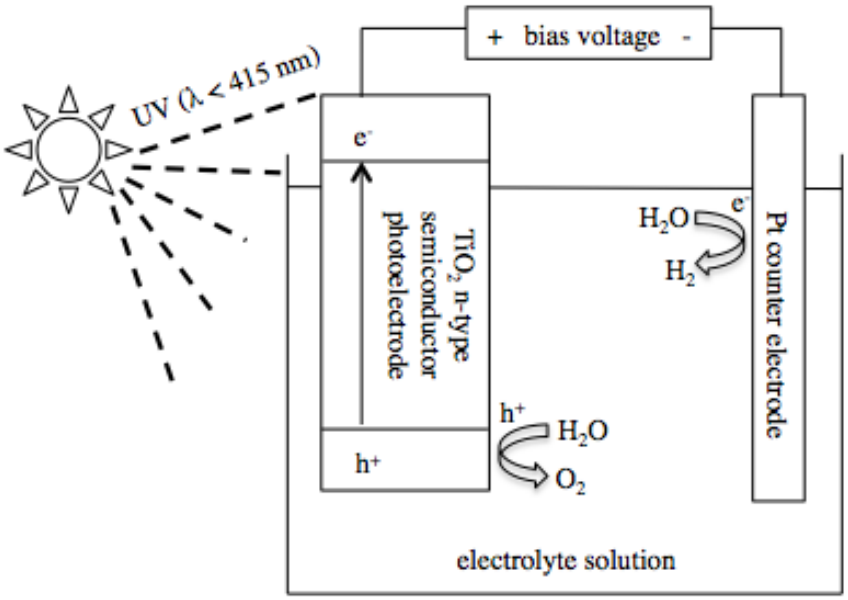

Figure 7. Honda-Fujishima photoelectrochemical solar water splitting cell using a TiO_2 photoelectrode.

The configuration and mechanism of photoelectrochemical water splitting cell consisting of two separate electrodes is presented in Figure 8. Upon light irradiation, the electron-hole pairs are generated in the semiconductor. The photogenerated holes migrate to the semiconductor surface and oxidize the adsorbed water molecules into oxygen. The photogenerated electrons are promoted into the conduction band and transferred to the metal cathode by applied voltage for water reduction. [1] [2] [3] [7] [8]

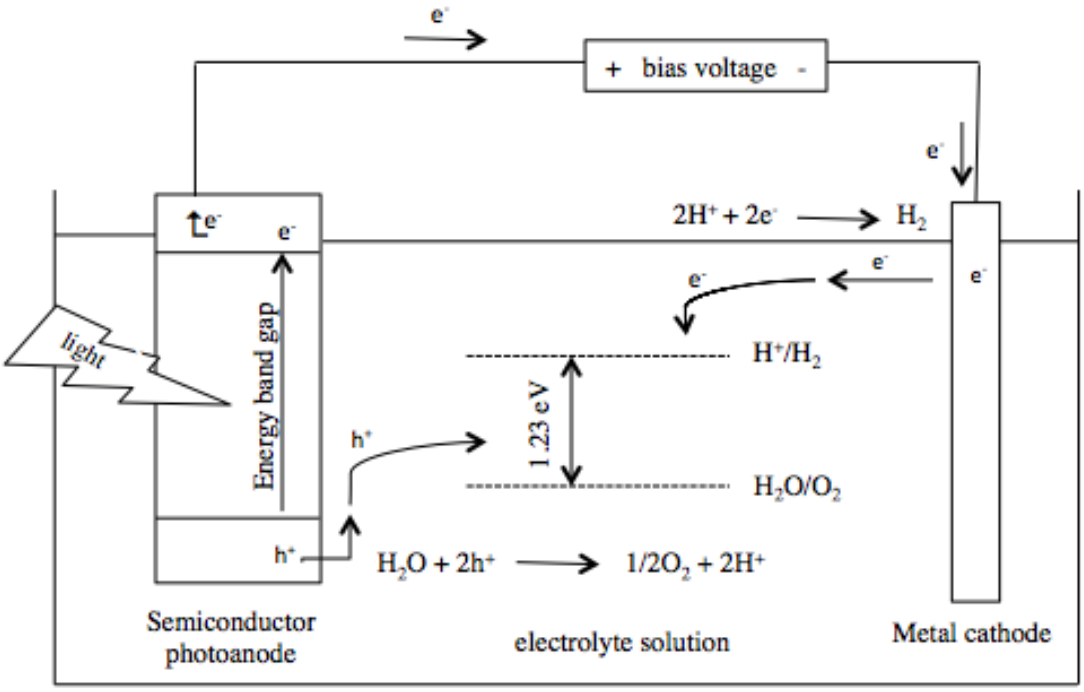

Figure 8. Solar water splitting by two separated electrodes assisted by a bias voltage.

Platinum is usually employed as the metal cathode in solar water splitting cells because it is non-reactive and resistant to corrosion. The development of photoanode remains challenging. The ideal properties of the photoanode include sufficiently small band gap to absorb significant portion of the solar spectrum, appropriate valence band level relative to water oxidation, effective charge separation and migration to surface reaction sites, stability under photo-oxidation reaction and aqueous condition, and low cost. [1] [3]

1.4 Ag_3PO_4 FOR SOLAR WATER SPLITTING

Recently, Yi et al. reported the use of silver phosphate (Ag_3PO_4) as a photocatalyst under visible light irradiation. Ag_3PO_4 was found to be able to harness visible light to oxidize water and decompose organic compounds. [11] [15] [16] [17] Figure 9 compares the oxygen evolution from aqueous $AgNO_3$ solutions under visible light illumination on various semiconductor powders, where water is oxidized to oxygen and $AgNO_3$ (used as a sacrificial agent) is reduced to Ag. It is apparent that Ag_3PO_4 shows much higher photo-oxidative efficiency compared to $BiVO_4$ and WO_3, two of the most efficient photocatalysts under visible light illumination known to date. Here, a sacrificial agent is used because the electrode potential of Ag_3PO_4 is below the water reduction potential which means that Ag_3PO_4 cannot reduce water to H_2 without the help from an applied voltage or a sacrificial agent. Ag_3PO_4 has also been used in photoelectrochemical cells for water splitting and shows promising efficiencies under visible light. The high photo-oxidative activity of Ag_3PO_4 under visible irradiation is attributed to its band structure. Ag_3PO_4 has a band gap of 2.4 eV which is suitable for absorption of visible light (Figure 10). [27] [28] [29]

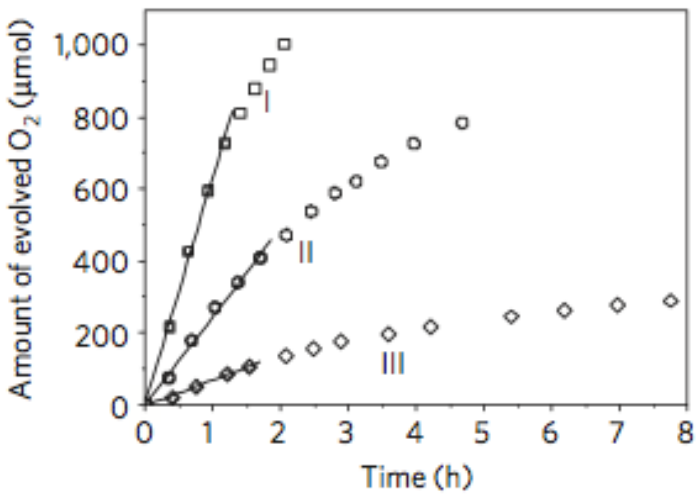

Figure 9. O_2 evolution from aqueous $AgNO_3$ solutions under illumination (> 400 nm) on various semiconductor powders (I) Ag_3PO_4: 636 mol/h (II) $BiVO_4$: 246 mol/h (III) WO_3: 72 mol/h. [11]

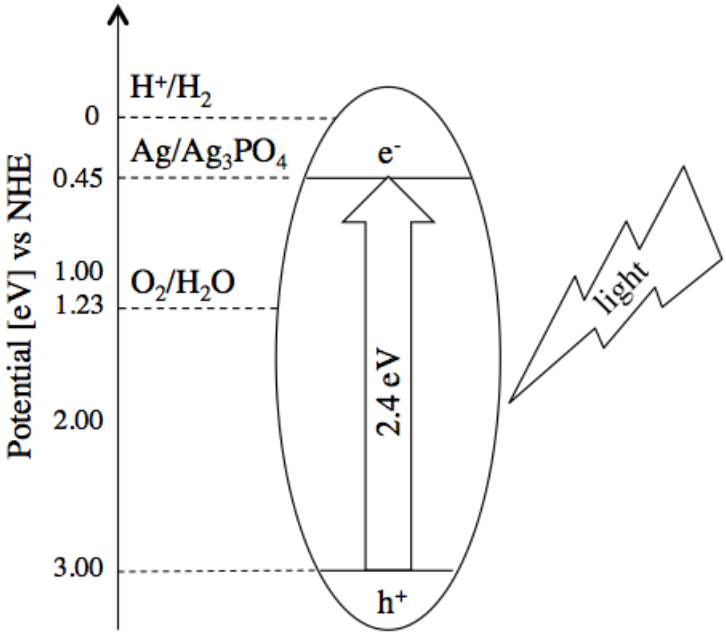

Figure 10. Schematic drawing of the band structure of Ag_3PO_4.

1.5 Ag_3PO_4 NANOPARTICLES AS PHOTOANODES FOR SOLAR WATER SPLITTING

As previously mentioned, the holes generated upon light illumination need to travel to the reaction sites on the surface of the photoanodes in order to oxidize water. On their path to the reaction sites, the photogenerated charge carriers can be trapped by various kinds of crystal defects and recombine. Decreasing the size of the photoanode material into nanometer ranges reduces the distance that the photogenerated charges need to travel to reach the reaction sites, and therefore reduces the recombination probability and improves the efficiency.

During the past few years, various efforts have been explored to synthesize Ag_3PO_4 nanoparticles. By controlling the size and morphology of the nanoparticles, the photocatalytic activity can be improved due to the decrease in charge diffusion length and increase in surface area. [1] [2] The study shows that Ag_3PO_4 nanoparticles have higher photocatalytic activity under visible light irradiation compared to micrometer-sized Ag_3PO_4 particles. [16] [20] [21]

Although Ag_3PO_4 nanoparticles promotes the holes transport to the reaction sites on their surface, the electrons have to hop between the nanoparticles in order to reach the external circuit and be transported to the cathode. Hopping between the nanoparticles increases the probability of the electrons to recombine with the holes on the surface and thus decreases the overall efficiency of the photoanode in water splitting. As a result, only very thin films of Ag_3PO_4 nanoparticles may be used as the photoanode, and above a certain thickness, thicker films of Ag_3PO_4 nanoparticles lead to decreased efficiency although thicker films may improve the light absorption.

Vertically ordered 1-D nanostructures have been used to promote electron transport in solar cells and batteries by providing a direct pathway for the electrons. Recently, my research group has developed processes for synthesizing vertically ordered long ZnO nanowires and has used them in dye-sensitized solar cells (DSSC). Xu et al. has reported high-efficiency DSSCs composed of multilayer ZnO nanowire arrays coated with TiO_2 nanoparticles as photoanodes. The vertically aligned 1-D nanostructures significantly improve performance of the DSSCs by promoting electron transport and facilitating filling of the films with solid and viscous hole-transporting materials. [10] [12] [13] [14]

Inspired by the employment of vertically ordered ZnO nanowires in DSSCs, in this thesis, I explore the use of composite photoanodes consisting of Ag_3PO_4 nanoparticles embedded into ZnO nanowire arrays for photoelectrochemical solar water splitting. The composite photoanode will take advantage of both the high photocatalytic activity of Ag_3PO_4 nanoparticles and the fast electron transport enabled by vertically ordered single crystalline ZnO nanowire arrays. Such Ag_3PO_4 nanoparticles-embedded ZnO nanowire array is expected to be a promising photoanode for solar water splitting.

2.0 RESEARCH OBJECTIVE

In this work, a composite photoanode consisting of Ag_3PO_4 nanoparticles embedded into ZnO nanowire arrays is fabricated for photoelectrochemical solar water splitting. The composite photoanode takes advantage of both the high photocatalytic activity of Ag_3PO_4 nanoparticles and the fast electron transport enabled by single crystalline ZnO nanowires.

ZnO nanowires and Ag_3PO_4 nanoparticles will be synthesized and characterized. Ag_3PO_4 nanoparticles will be embedded into ZnO nanowire arrays by spin coating. The photo-oxidation activity of the Ag_3PO_4 nanoparticle-embedded ZnO nanowire arrays will be investigated. Photoelectrochemical cells for water splitting will be fabricated. Current densities as a function of externally applied voltage will be measured upon light irradiation. Ag_3PO_4 nanoparticle-embedded ZnO nanowire arrays will be compared with films of Ag_3PO_4 nanoparticles deposited on a thin ZnO film, when both used as the photoanode for water splitting.

We will also verify the hypothesis that embedding the Ag_3PO_4 nanoparticles into ordered ZnO nanowire arrays may allow much thicker films of Ag_3PO_4 nanoparticles to be used and the photocurrent may be significantly improved compared to planar Ag_3PO_4 /ZnO films

3.0 EXPERIMENT

3.1 ZnO NANOWIRES AND PLANAR ZnO PREPARATION

3.1.1 Materials

Zinc nitrate ($Zn(NO_3)_2$), polyethyleneimine (PEI, end-capped, molecular weight 800 g/mol) and hexamethylenetetramine (HMTA) were obtained from Sigma-Aldrich. Ethanol and ammonium hydroxide (NH_4OH) were obtained from Pharmco-AAPER and J.T.Baker, respectively. The indium doped-tin oxide (ITO) glass substrate was obtained from Precision Glass & Optics.

3.1.2 Methods

The growth of ZnO nanowire arrays was based on the method developed by Xu et al. [12] Briefly, the ITO glass substrate of 5 cm^2 was first cleaned by sonication in acetone and ethanol for 20 min, followed by treatment in ultraviolet ozone cleaner (Jelight) for 30 min. The substrate was then spin-coated with 5 mM of zinc acetate solution in ethanol, followed by thermal treatment at 150°C for 2 min. The substrate was spin-coated another time, followed by thermal treatment at 350°C for 30 min. The thermal treatment decomposed zinc acetate to zinc oxide nanocrystals on the substrate, which were used as seeds for subsequent ZnO nanowires growth.

The growth solution consisted of 0.05 M $Zn(NO_3)_2$, 0.025 M HMTA, 0.005 M PEI and 0.45 M NH_4OH. The seeded substrate was faced down in the bottle containing 30 ml of growth solution. The container was covered and placed in the preheated, 87-89°C, water bath to start the growth of ZnO nanowires. It took 30 - 45 min to observe the white layer of ZnO on the substrate. After 3 hr, the obtained ZnO nanowire arrays on ITO glass substrate were rinsed with DI water and calcined in air at 450°C for 30 min to remove any organic residuals. Figure 11 shows the schematic of ZnO nanowire synthesis process. The pH of the growth solution measured before and after the growth process are 10.5 and 10.3, respectively.

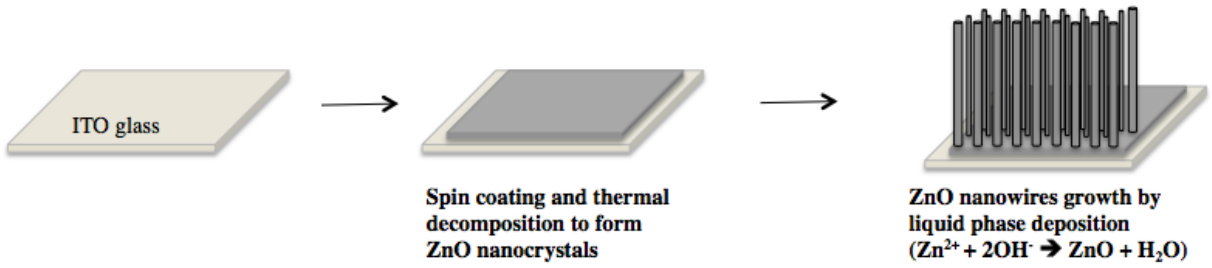

Figure 11. Schematic of ZnO nanowire array synthesis process.

Planar ZnO film was synthesized by using the same method for synthesizing the ZnO seed layers. The ITO glass substrate was spin-coated with 5 mM of zinc acetate solution in ethanol, followed by thermal treatment at 150°C for 2 min. Then, the substrate was spin-coated another time and thermal treated at 350°C for 30 min to decompose zinc acetate to zinc oxide nanocrystals.

3.2 Ag_3PO_4 NANOPARTICLES PREPARATION

3.2.1 Materials

Silver nitrate ($AgNO_3$) and toluene were obtained from Post Apple Scientific and J.T. Baker, respectively. Phosphoric acid (H_3PO_4) and oleylamine (OM) were obtained from Sigma-Aldrich. Absolute ethanol was obtained from Pharmco-AAPER.

3.2.2 Methods

The synthesis of Ag_3PO_4 nanoparticles is based on the study of Dinh et al. as represented in Figure 12. [21] For synthesis of approximately 2 grams of Ag_3PO_4; 2 mmol of $AgNO_3$ and 4 mmol of OM were dissolved in 6 ml of toluene. $AgNO_3$ can be slowly dissolved in OM at room temperature; for example, 50 mg of $AgNO_3$ was reported to take 1 hr to dissolve in 2 ml of OM. [23] To this solution, the mixture of 2 mmol H_3PO_4 dissolved in 2 ml of absolute ethanol was gradually added into the solution. The color of the solution slowly changed from colorless to yellow, indicating the formation of Ag_3PO_4. After 30 min of stirring, excess ethanol was added into the solution to precipitate Ag_3PO_4 nanoparticles. Then the obtained nanoparticles were re-dispersed in toluene and re-precipitated in ethanol. The washing process was done several times to remove all unreacted reagents and excess OM. Figure 12 shows the schematic of Ag_3PO_4 nanoparticles synthesis process.

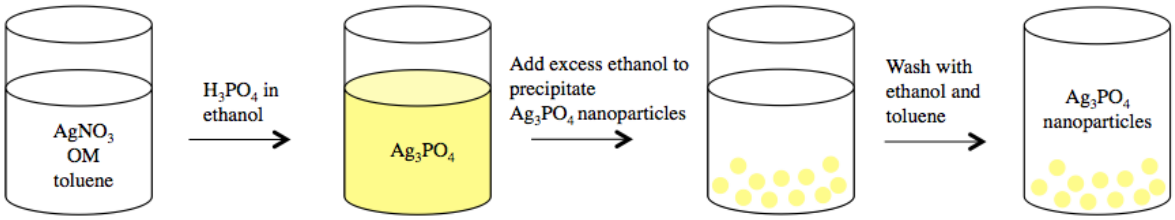

Figure 12. Schematic of Ag_3PO_4 nanoparticles synthesis process.

3.3 DEPOSITION OF Ag_3PO_4 NANOPARTICLES ONTO ZnO NANOWIRE ARRAYS AND PLANAR ZnO FILM

3.3.1 Methods

0.4 mmol of Ag_3PO_4 nanoparticles were re-dispersed in 1 ml of toluene. The mixture was then sonicated for 1 hr. After sonication, 10 µl of the Ag_3PO_4-dispersed in toluene was spin-coated onto ZnO nanowire arrays and planar ZnO film. Figure 13 represents the schematic for depositing Ag_3PO_4 nanoparticles onto ZnO nanowire arrays and planar ZnO film. The Ag_3PO_4 nanoparticle-embedded ZnO nanowire arrays and planar Ag_3PO_4/ZnO films were then calcined in air at 450°C for 30 min to remove any organic residuals.

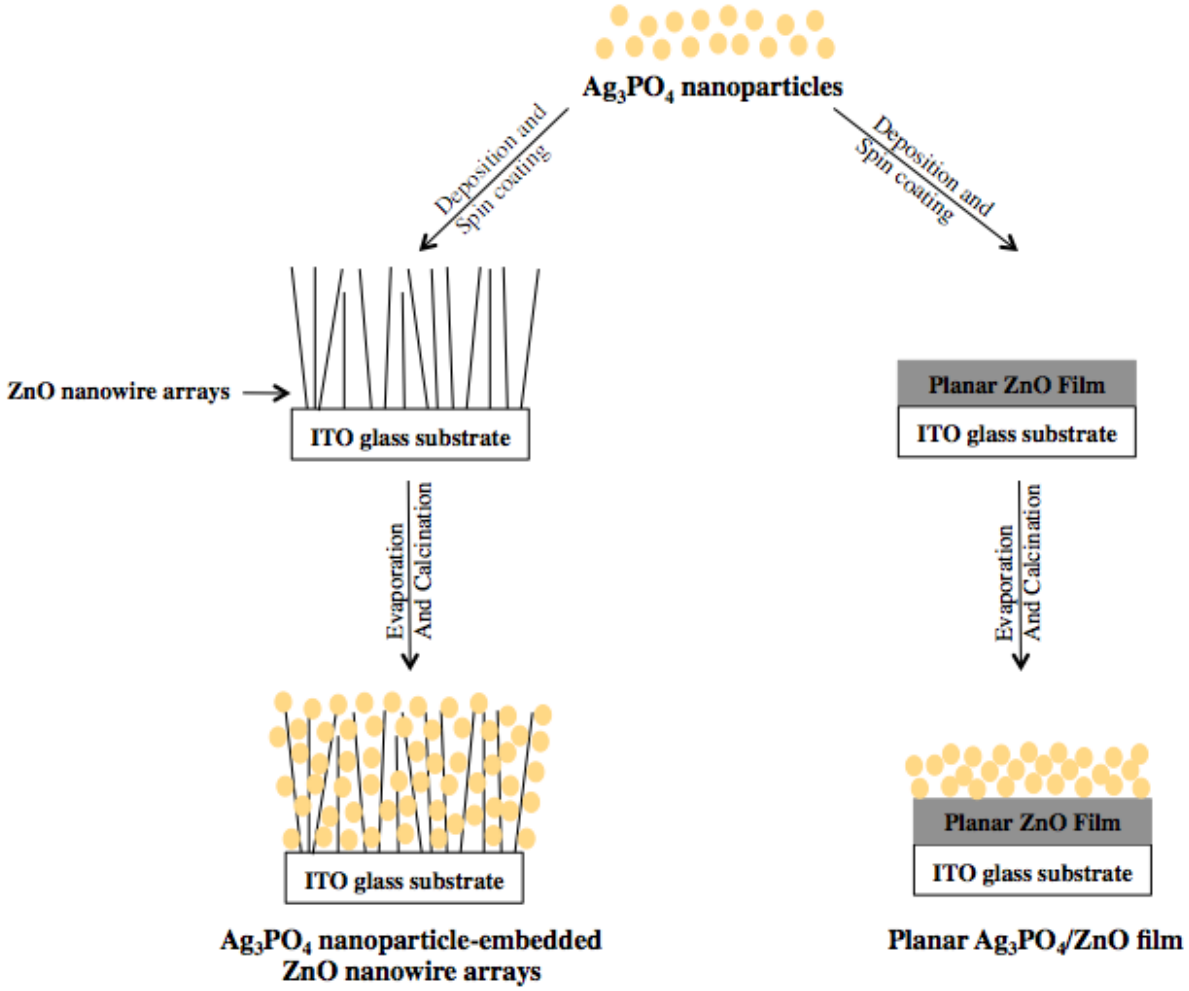

Figure 13. Schematic diagram for the deposition of Ag_3PO_4 nanoparticles onto ZnO nanowire arrays and planar ZnO films.

3.4 CHARACTERIZATION

Scanning electron microscopy (SEM) images were taken using a field-emission electron microscope (Philips XL). The X-ray diffraction (XRD) spectra were taken by Philips X'pert diffractometer. UV-Vis absorption spectra were taken on a DU700 spectrophotometer (Beckman

Coulter). The spectra were scanned from 300 to 800 nm wavelength. The elemental analysis was performed by energy dispersive X-ray spectroscopy (Philips XL-30 EDS, EDAX).

3.5 PHOTO-OXIDATION ACTIVITY MEASUREMENT

The photo-oxidation activities of the Ag_3PO_4 nanoparticle-embedded ZnO nanowire arrays and planar Ag_3PO_4/ZnO films were determined by the linear voltametry upon light irradiation by using the three-electrode cell configuration and with Reference 600 Potentiostat (Gamry Instruments). Pt coil and Ag/AgCl electrode (accumet, Fisher Scientific) and 1 M KOH were used as counter electrode, reference electrode, and electrolyte, respectively. Linear sweep voltammograms were collected at 5 mV/s. The light source was 200 W Xe lamp (Newport). The distance from the lamp to the sample was kept constant at 45 cm. The light intensity was 100 mW/cm^2 as measured by high sensitivity thermopile sensor and optical power and energy meter (OPHIR). Figure 14 shows the experimental setup for photo-oxidation measurement.

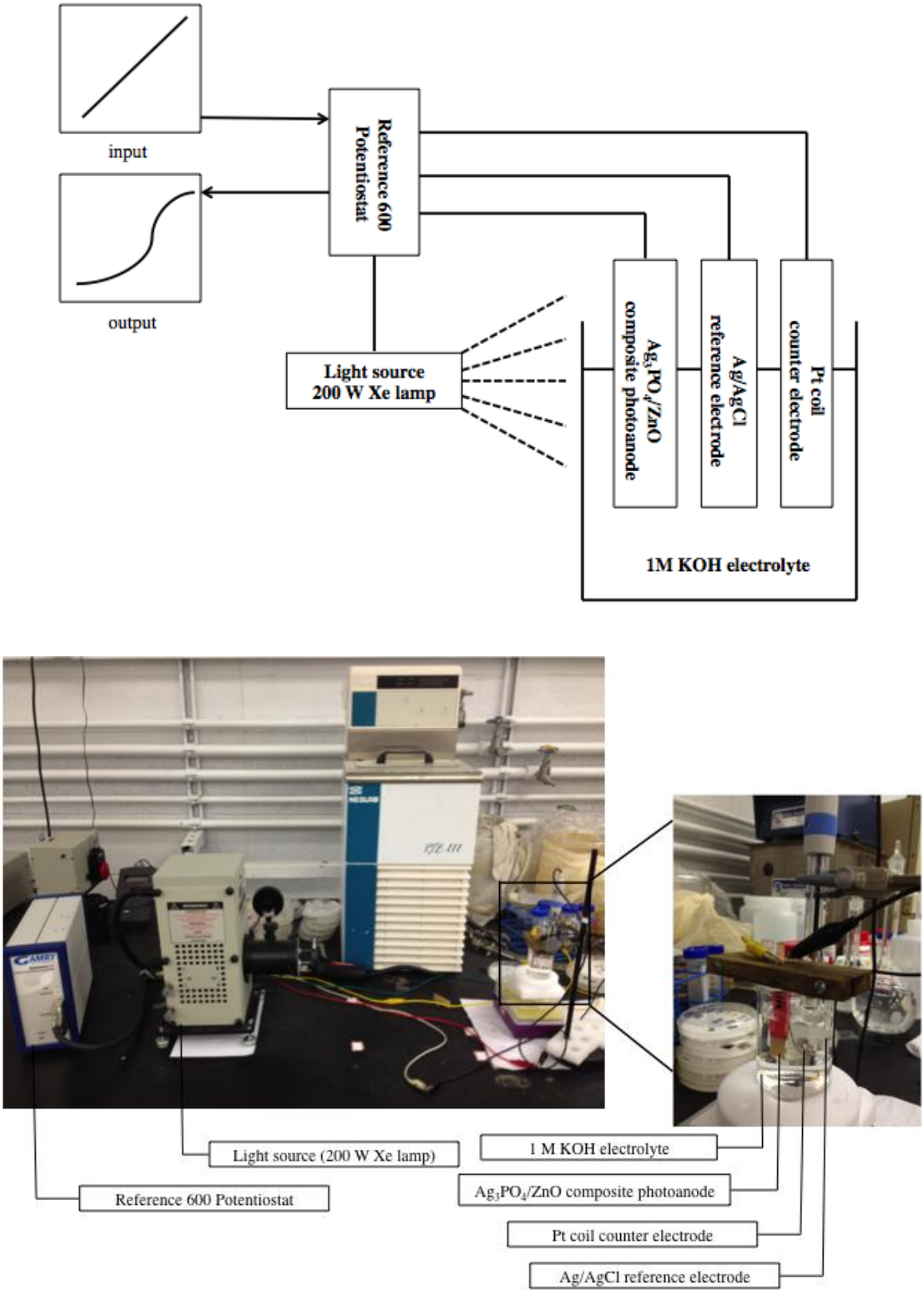

Figure 14. Experimental setup for photo-oxidation measurement.

4.0 RESULTS AND DISCUSSION

4.1 ZnO NANOWIRE ARRAYS

ZnO nanowire arrays were synthesized by the liquid phase deposition (LPD) method by the following reaction:

$$Zn^{2+} + 2OH^- \rightarrow ZnO + H_2O \quad (4.1),$$

where HMTA served as a hydroxide source. The advantages of LPD method are low growth temperature, low cost and easy to scale up. However the ZnO nanowires, synthesized by LPD approach, tend to form in bulk solution and on the seeded substrate simultaneously, resulting in low growth rate from rapid depletion of reactants and contamination of nanowires from floating substance.

In this work, the ZnO nanowire arrays were prepared with the couple use of NH_4OH and PEI. NH_4OH forms the complex with zinc ions (Zn^{2+}) to lower the supersaturation of the growth solution, preventing the homogeneous nucleation process in bulk solution. PEI adsorbs to certain crystal faces of ZnO, preventing the growth of ZnO along those faces by steric hindrance. However, the crystal sizes on the pre-seeded substrate are large enough that they are not affected by the presence of PEI. Therefore, ZnO is still growing on the seeded substrate. With this process, the growth of ZnO is entirely on the substrate without the formation of ZnO precipitate in bulk solution. [12]

Figure 15 shows the SEM images of the synthesized ZnO nanowire arrays. The average lengths of nanowires are 7.5 μm and the diameter is approximately 0.5 μm.

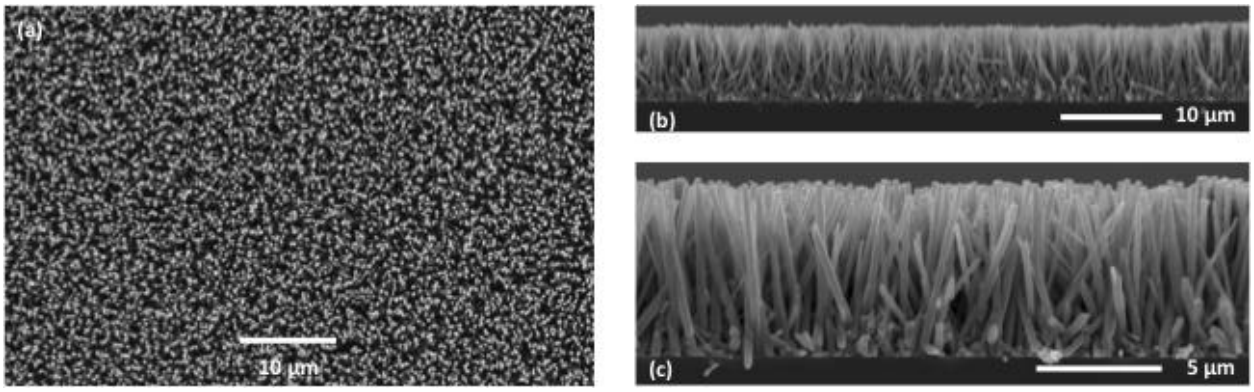

Figure 15. SEM images of ZnO nanowires, (a) top-view; (b) and (c) cross-sectional view.

Figure 16 presents the XRD pattern of the synthesized ZnO nanowires. The peaks are assigned according to JCPDS card no. 36-1451. A strong and dominant peak corresponding to the (002) orientation indicates that the ZnO nanowires are well oriented along the substrate surface, which is consistent with the SEM images. [24] [25] [26]

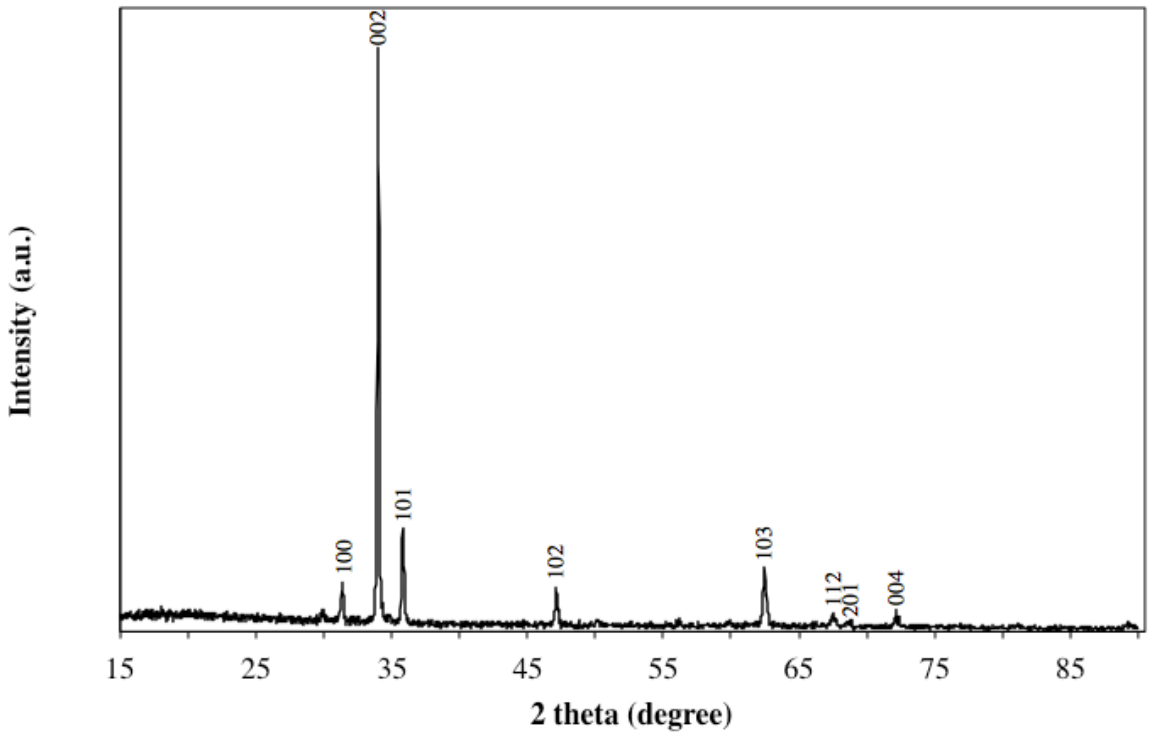

Figure 16. XRD pattern of ZnO nanowire arrays.

4.2 Ag_3PO_4 NANOPARTICLES

The Ag_3PO_4 nanoparticles were synthesized by the reaction between H_3PO_4 and silver ions (Ag^+) with OM, used as a surface-capping agent. The OM coating on the nanoparticle surface is formed by the acid-base interaction between H_3PO_4 and OM. In the presence of OM, uniform Ag_3PO_4 nanoparticles are formed because OM molecules play an important role in preventing the agglomeration of nanoparticles by providing a repulsive force opposing van der Waals attraction between the nanoparticles. The capping OM molecules are weakly bonded to the Ag_3PO_4 nanoparticles surface; therefore, they can be removed or modified easily. [23]

A SEM image of Ag_3PO_4 nanoparticles dispersed in ethanol is shown in Figure 17. The diameter of the particles is approximately 40 nm.

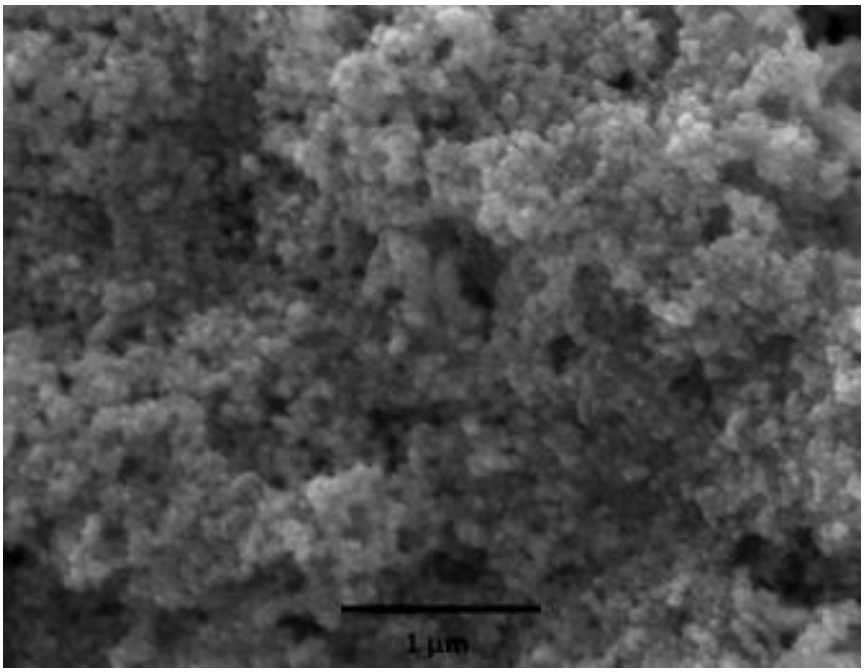

Figure 17. SEM image of Ag_3PO_4 nanoparticles dispersed in ethanol.

The XRD pattern of pure Ag_3PO_4 is displayed in Figure 18. The diffraction peaks can be indexed to the various planes of body-centered cubic of Ag_3PO_4 (JCPDS no. 06-0505). [18] [19] [20]

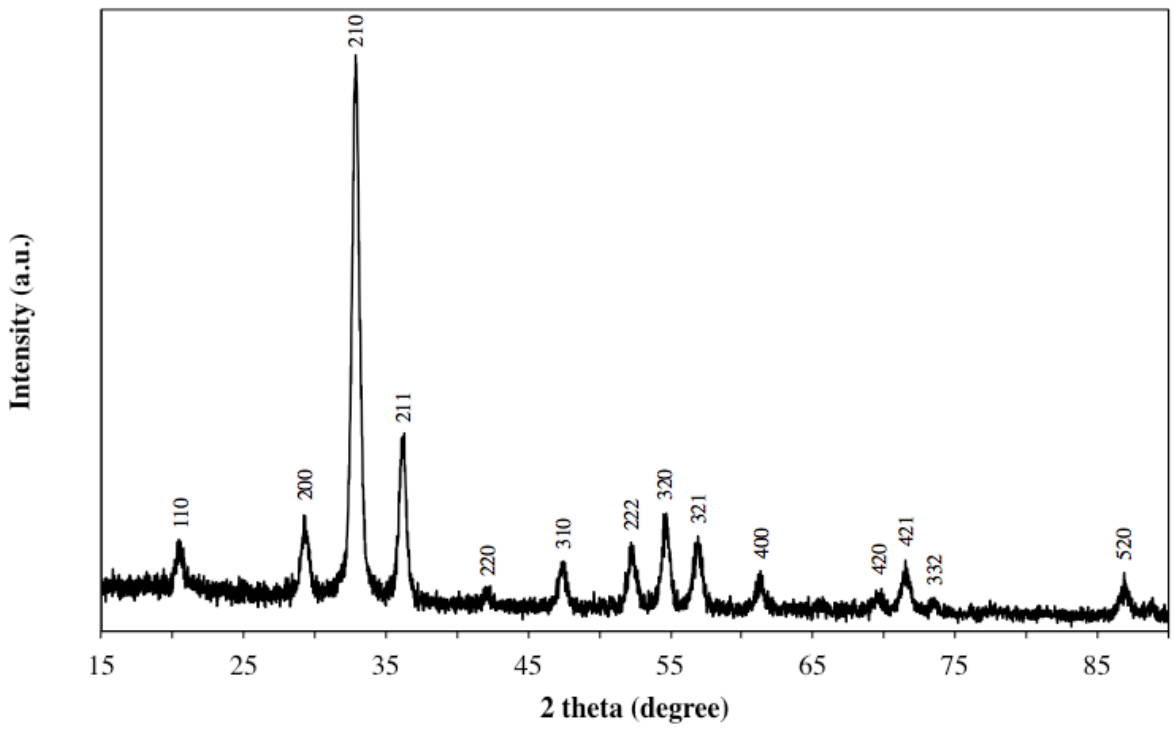

Figure 18. XRD pattern of Ag_3PO_4 nanoparticles.

Figure 19 shows the UV-Vis diffuse reflectance spectrum of Ag_3PO_4 nanoparticles dispersed in toluene. Ag_3PO_4 absorbs light with a wavelength shorter than 502 nm, corresponding to its 2.4 eV band gap.

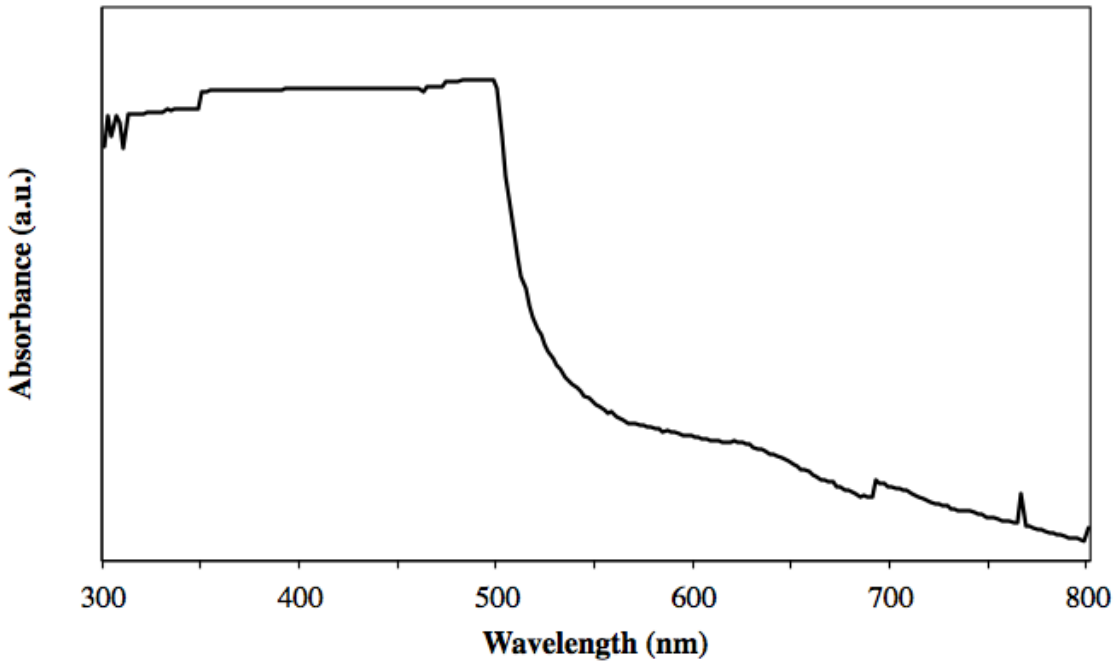

Figure 19. UV-visible diffuse reflectance spectrum of Ag_3PO_4 nanoparticles dispersed in toluene.

4.3 Ag_3PO_4 NANOPARTICLE-EMBEDDED ZnO NANOWIRE ARRAYS AND PLANAR Ag_3PO_4/ZnO FILMS

The deposition of Ag_3PO_4 nanoparticles consists of dropping the Ag_3PO_4 nanoparticles solution in reasonable amount, spinning and drying. The solution dropped on top of ZnO nanowires serves as a reservoir during the deposition process. [13] Figure 20 shows SEM images of Ag_3PO_4 nanoparticle-embedded ZnO nanowire arrays, demonstrating that Ag_3PO_4 nanoparticles are filling the space between nanowire arrays with small overlayer.

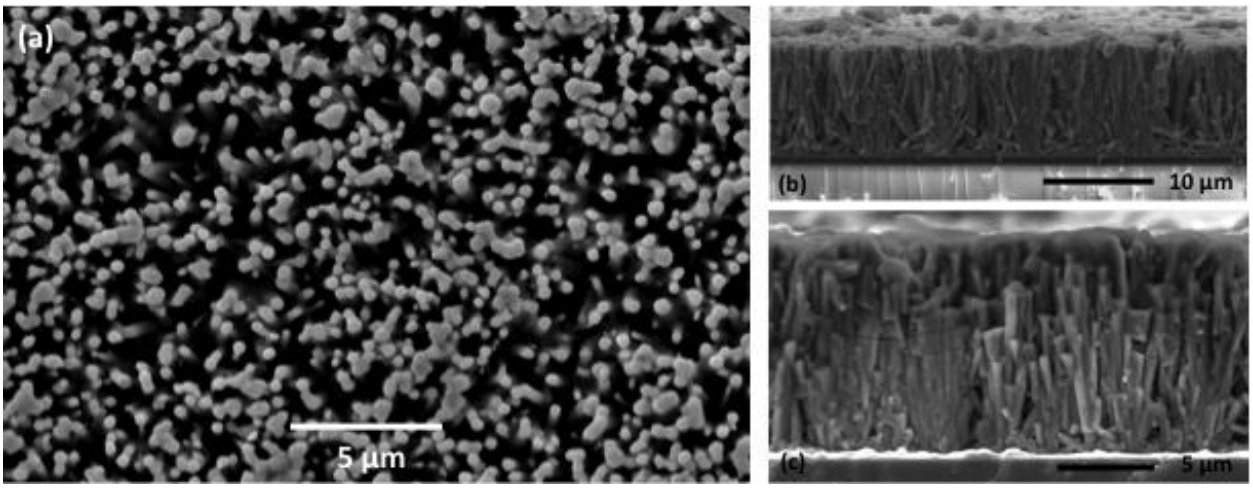

Figure 20. SEM images of Ag_3PO_4 nanoparticle-embedded ZnO nanowire arrays, (a) top-view; (b) and (c) cross-sectional view.

Figure 21 compares the XRD patterns of Ag_3PO_4 nanoparticle-embedded ZnO nanowire arrays with ZnO nanowires and Ag_3PO_4 nanoparticles. Diffraction peaks from both ZnO nanowires and Ag_3PO_4 nanoparticles have been detected on the XRD pattern of Ag_3PO_4 nanoparticle-embedded ZnO nanowire arrays, confirming that the Ag_3PO_4 nanoparticles have been embedded into the ZnO nanowire arrays.

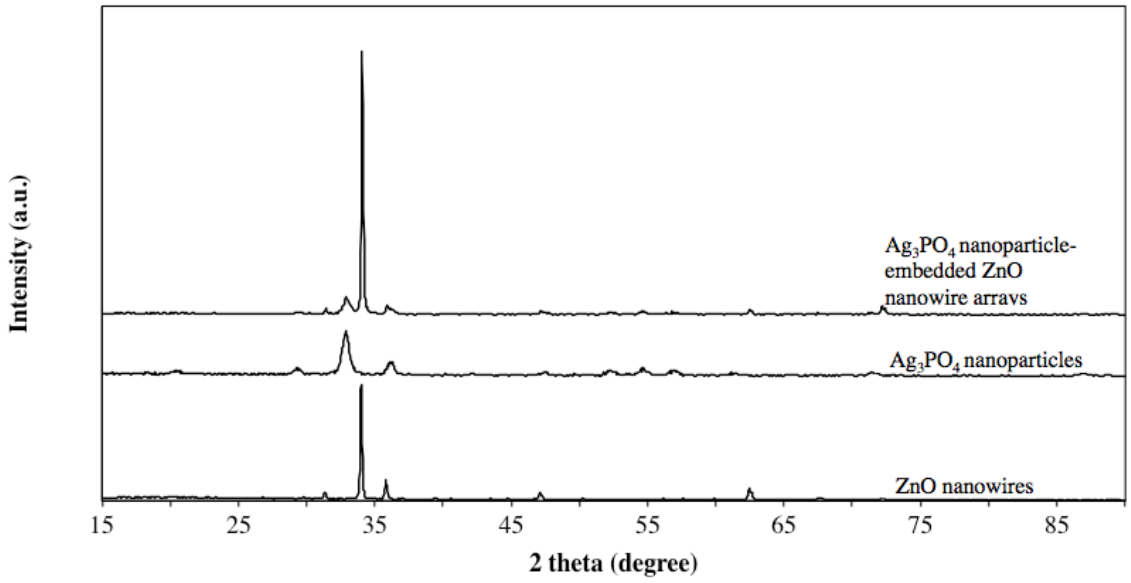

Figure 21. XRD patterns of ZnO nanowires, Ag_3PO_4 nanoparticles, and Ag_3PO_4 nanoparticle-embedded ZnO nanowire arrays.

The energy dispersive X-ray spectroscopy (EDX) spectrum of the Ag_3PO_4 nanoparticle-embedded ZnO nanowire arrays is shown in Figure 22. The peaks from O, Zn, P and Ag further confirm the presence of both Ag_3PO_4 and ZnO.

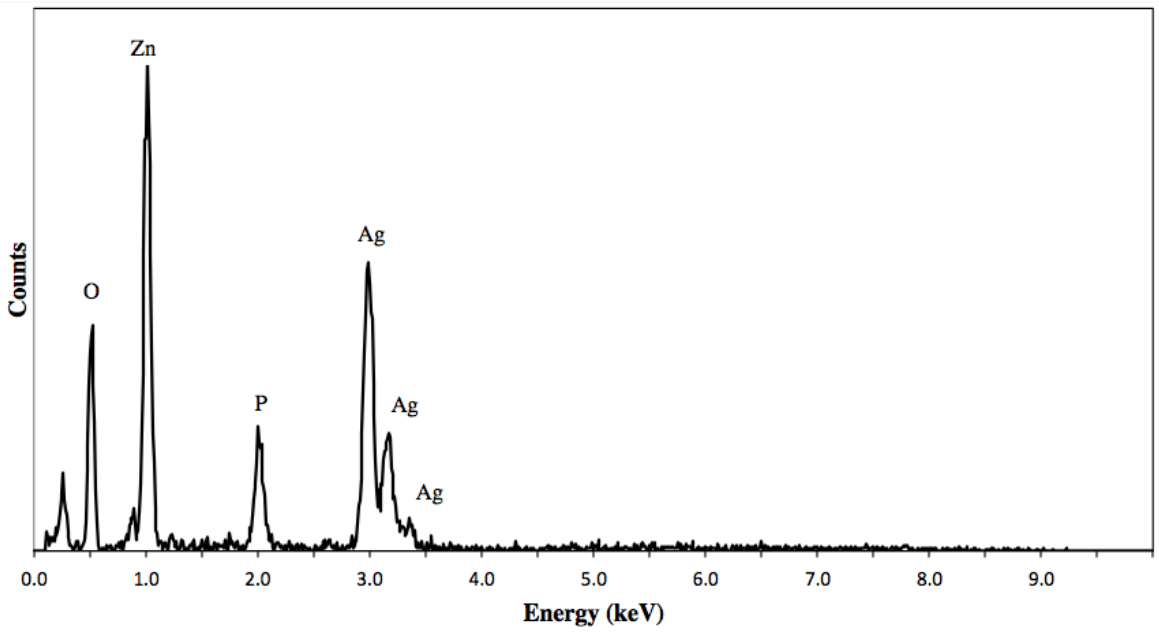

Figure 22. EDX spectrum of Ag_3PO_4 nanoparticle-embedded ZnO nanowire arrays.

Figure 23 shows the XRD pattern of films of Ag_3PO_4 nanoparticles deposited onto a planar ZnO thin film, with XRD patterns of ZnO nanowires and Ag_3PO_4 nanoparticles. [31] [32]

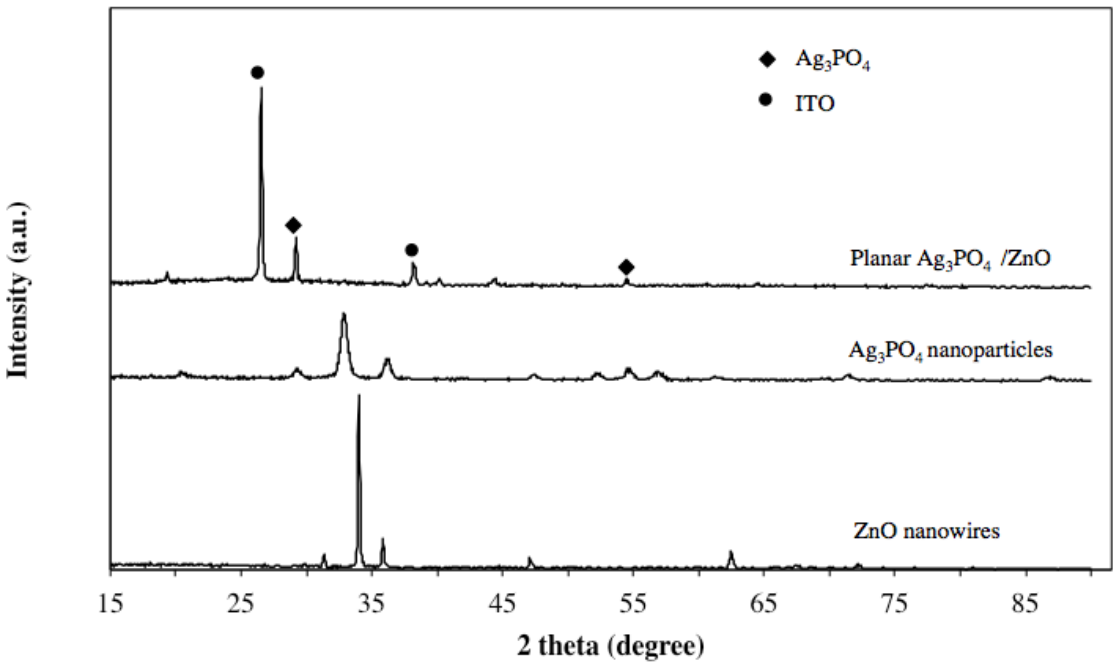

Figure 23. XRD patterns of ZnO nanowires, Ag_3PO_4 nanoparticles, and planar Ag_3PO_4/ZnO.

4.4 THE PHOTO-OXIDATION ACTIVITY MEASUREMENT

The performance of the Ag_3PO_4/ZnO composite photoanode was studied by linear sweep voltammetry. An external bias voltage was applied to the cell in order to compensate the potential difference between the redox potential and the potential required to transfer the photogenerated electrons to the Pt cathode. Under light irradiation, the photogenerated holes migrated to the interface between the Ag_3PO_4 nanoparticles and the electrolyte, and oxidized water to produce oxygen. Photogenerated electrons were excited to the conduction band and transferred to the external circuit through the ZnO nanowires. After running through the external circuit, the electrons were transported to the Pt cathode and reduced water to produce hydrogen. The schematic representation of the water oxidation at Ag_3PO_4 nanoparticle-embedded ZnO nanowire arrays photoanode and water reduction at Pt cathode is depicted in Figure 24.

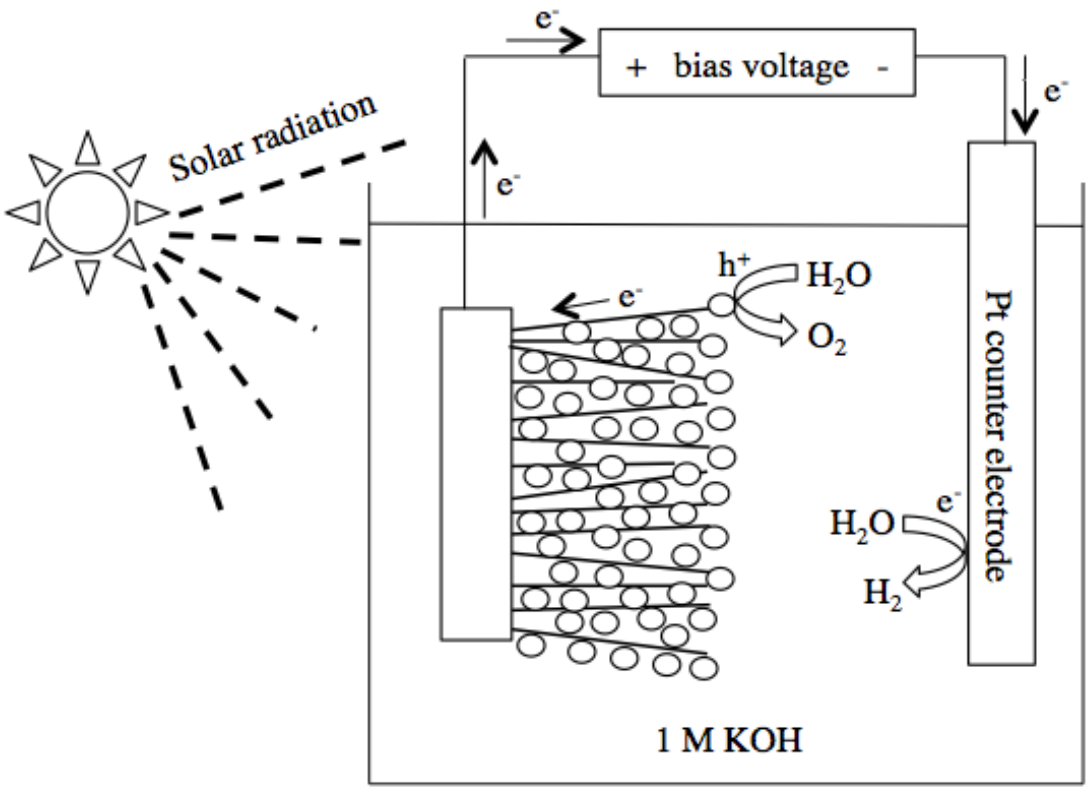

Figure 24. Schematic of photoelectrochemical solar water splitting by using Ag_3PO_4 nanoparticle-embedded ZnO nanowire arrays as photoanode and Pt as counter electrode.

Figure 25 presents the current density versus potential (*J-V*) curve for the water splitting cell that uses Ag_3PO_4 nanoparticle-embedded ZnO nanowire arrays as the photoanode under visible light illumination, and compares it with the *J-V* curve in dark. The photocurrent under light illumination is much higher than in dark, confirming the photo-oxidation activity of the photoanode. The onset potential of the Ag_3PO_4 nanoparticle-embedded ZnO nanowire arrays is below 0.1 V (versus V_{ref}).

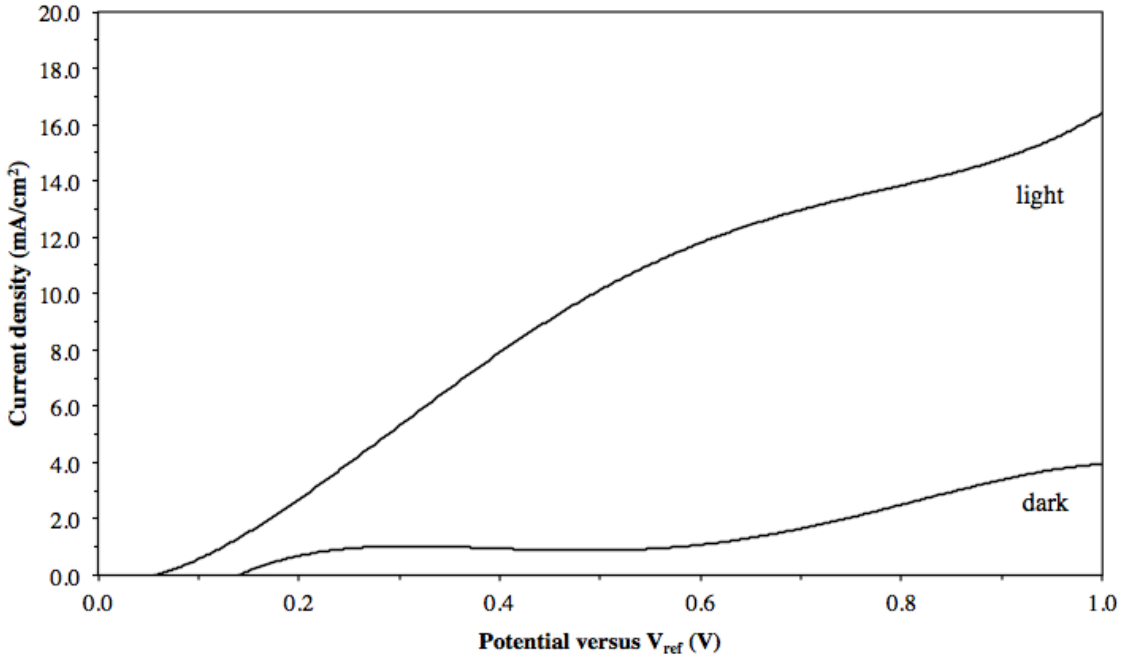

Figure 25. Current density versus potential for Ag_3PO_4 nanoparticle-embedded ZnO nanowire arrays photoanode with light illumination and in dark.

As a comparison, photoanodes were also fabricated by depositing Ag_3PO_4 nanoparticle films on a very thin planar ZnO film, and the thickness of the films were varied from 0.4 to 1.5 μm. *J-V* curves of the water splitting cells that use these photoanodes with different thicknesses of the Ag_3PO_4 films were measured and presented in Figure 26. In principle, increasing the thickness of Ag_3PO_4 nanoparticle films increases the surface areas for the water oxidation reaction which takes place at the Ag_3PO_4/electrolyte interface, and one would expect an increase in the photocurrent as the film thickness increases. However, it is observed that as the thickness of the Ag_3PO_4 nanoparticle films increases from 0.4 to 1 and then to 1.5 μm, the photocurrent density significantly decreases. This is likely because when the Ag_3PO_4 film thickness increases, transport of electrons from the Ag_3PO_4 nanoparticles to the external circuit becomes less efficient and eventually becomes the bottleneck for the water splitting process. Significant

percentages of the electrons are not able to travel to the external circuit before they recombine with the photogenerated holes. Only those electrons close to the bottom ZnO layer are able to move to the external circuit, but photogenerated electrons at the top surface of the film where light is absorbed the most are not able to travel to the external circuit. As a result, as the film thickness increases, the number of electrons generated at the bottom layer of the film, which are close enough to the conducting layer to move to the external circuit, decreases because the Ag_3PO_4 nanoparticles in the bottom layer are illuminated with less light. This result clearly illustrates the importance of charge transport in determining the efficiency of the photoanode in water splitting process.

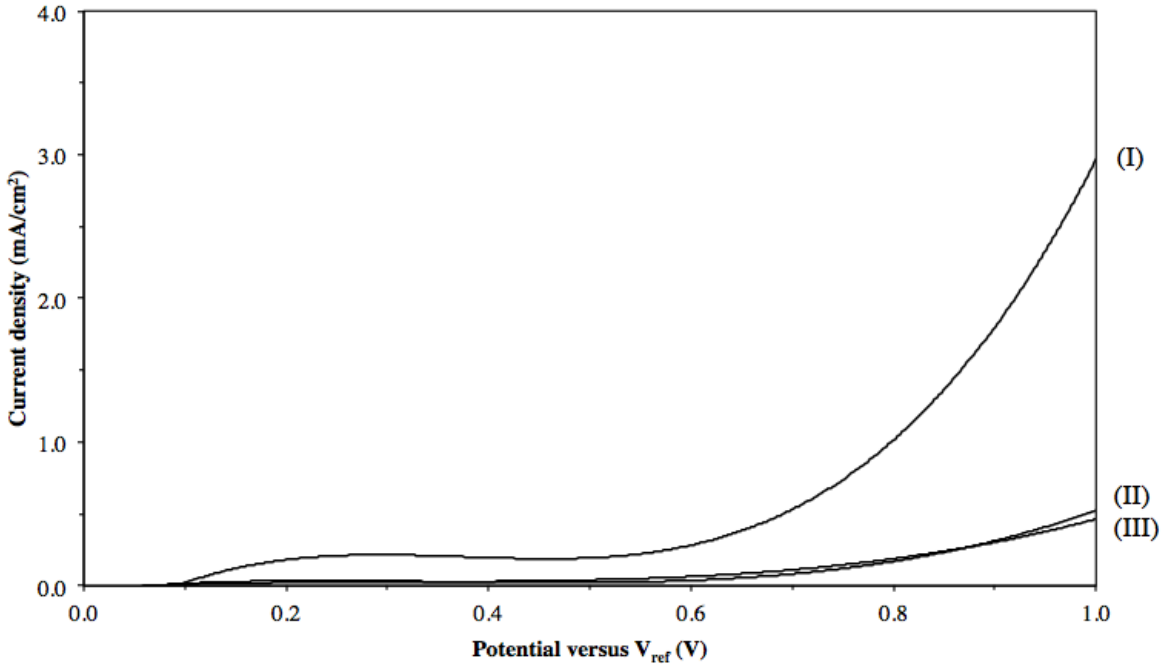

Figure 26. Current density versus potential curves for planar Ag_3PO_4/ZnO films of (I) 0.4 μm thick, (II) 1.0 μm thick, and (III) 1.5 μm thick.

For further comparison, Ag_3PO_4 nanoparticles were also embedded on shorter ZnO nanowire arrays. Figure 27 compares the photocurrents from the photoanodes made of Ag_3PO_4

nanoparticle-embedded ZnO nanowire arrays and planar Ag_3PO_4/ZnO films. It is apparent that the photoanodes made of Ag_3PO_4 nanoparticle-embedded ZnO nanowire arrays produces significantly higher current than the planar Ag_3PO_4/ZnO film photoanode. The highest photocurrent is achieved when ZnO nanowire array is about 7.5 μm in height. When embedded with Ag_3PO_4 nanoparticles, it produces 2 times higher current than 3.0 μm Ag_3PO_4 nanoparticle-embedded ZnO nanowire arrays, and 6 times higher current than the 0.4 μm thick planar Ag_3PO_4/ZnO film, and more than 15 times higher current than the 1 μm and 1.5 μm thick planar Ag_3PO_4/ZnO films. Use of ZnO nanowire arrays allows rapid transport of electrons from the Ag_3PO_4 nanoparticles to the external circuit through a direct pathway of single crystalline ZnO. Therefore, much thicker films of Ag_3PO_4 nanoparticles can be used at the anode, which means that more surface area of Ag_3PO_4 particles are available for the photo-activated water oxidation reaction, resulting in higher photocurrent. This result suggests promise of Ag_3PO_4 nanoparticle-embedded ZnO nanowire arrays as photoanodes for solar water splitting.

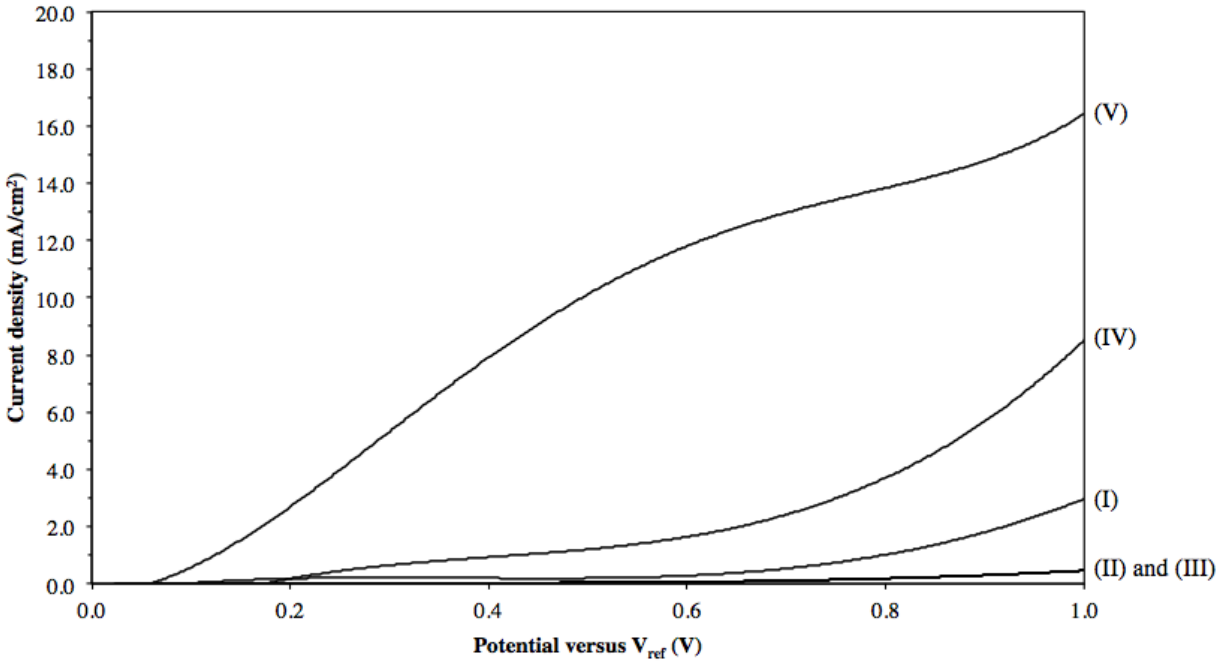

Figure 27. Comparison of the current density versus potential for (I-III) planar Ag_3PO_4/ZnO films of 0.4 μm thick, 1.0 μm thick, and 1.5 μm thick, respectively, and (IV-V) Ag_3PO_4 nanoparticle-embedded ZnO nanowire arrays of 3.0 μm height, and 7.5 μm height, respectively.

5.0 CONCLUSION

Solar water splitting is an attractive approach for production of renewable clean fuels. In this work, a new type of photoanodes consisting of Ag_3PO_4 nanoparticles embedded in ZnO nanowire arrays has been developed and characterized for photoelectrochemical water splitting. The composite photoanode takes advantage of both the high photocatalytic activity of Ag_3PO_4 nanoparticles under visible light illumination and the fast electron transport capability of single crystalline ZnO nanowires.

A process has been developed for fabrication of photoanodes made of Ag_3PO_4 nanoparticles embedded in ZnO nanowire arrays, which involves ZnO nanowire growth, synthesis of Ag_3PO_4 nanoparticles, and embedding of the Ag_3PO_4 nanoparticles into ZnO nanowire arrays by spin-coating. As a comparison, planar photoanodes have also been made by depositing films of Ag_3PO_4 nanoparticles in various thicknesses on a very thin ZnO film.

The photo-oxidation activities of both types of anodes, made of (i) Ag_3PO_4 nanoparticles embedded into ZnO nanowire arrays and (ii) Ag_3PO_4 nanoparticles deposited on a thin ZnO film, have been studied and compared. It is observed that without using the ZnO nanowire arrays, increasing the thickness of the Ag_3PO_4 nanoparticle films from 0.4 to 1 and to 1.5 μm leads to decrease of the efficiency, mainly due to less efficient transport of electrons hopping between the nanoparticles. On the contrary, by embedding the Ag_3PO_4 nanoparticles into the ZnO nanowire array, electrons can be transported to the external circuit through a direct pathway provided by

the single crystalline ZnO nanowires, thus enabling the use of much thicker films of Ag_3PO_4 nanoparticles. The thicker film provides more surface area for the photo-oxidation of water and leads to higher photocurrent. Through experiments, we have observed more than 6 times improvement in the photocurrent when Ag_3PO_4 nanoparticles are embedded into ZnO nanowires compared to when Ag_3PO_4 nanoparticles are deposited onto a planar ZnO film. Our result indicates that Ag_3PO_4 nanoparticles-embedded ZnO nanowire array is a promising composite photoanode for photoelectrochemical water splitting.

BIBLIOGRAPHY

[1] Sun J., Zhong, D.K. & Gamelin, D.R. Composite photoanodes for photoelectrochemical solar water splitting. *Energy Environ. Sci*. 3, 1252-1261 (2010).

[2] Kudo, A. & miseki, Y. Heterogeneous photocatalyst materials for water splitting. *Chem. Soc. Rev*. 38, 253-278 (2009)

[3] Choi, K.S. *Band Gap Tuning of Zinc Oxide Films for Solar Energy Conversion*. West Lafayette, Indiana: Department of Chemistry, Purdue University. Retrieved August 4, 2012, from http://papadanton akis.com/images/9/91/Band_Gap_Module

[4] Walter, M.G. et al. Solar water splitting cells. Chem. Rev. 110, 6446-6473 (2010).

[5] Ram, A. (2011, June 2). Solar and Heat Control Glasses. *The Glass Blog*. Retrieved August 4, 2012, from http://theglassblog.wordpress.com/2011/02/06/solar-and-heat-control-glasses/

[6] *Solar Energy*. Retrieved August 4, 2012, from http://www.resource-solar.com/resources/solar-energy

[7] Herrmann, J.M. Heterogeneous photocatalyst: fundamentals and applications to the removal of various types of aqueous pollutants. *Catalyst Today*. 53, 115-129 (1999).

[8] Gratzel, M. Photoelectrochemical cells. *Nature.* 414, 338-344 (2001).

[9] Fujishima, A. & Honda, K. Electrochemical photolysis of water at a semiconductor electrode. *Nature.* 238, 37-38 (1972).

[10] Peng, Q. & Qin, Y. (2011). *ZnO Nanowires and Their Application for Solar Cells*. Nanchang, China: Department of Environmental & Chemical Engineering, Nanchang Hangkong University. Retrieved August 4, 2012, from http://www.intechopen.com/books/nanowires-implementations-and-applications/zno-nanowires-and-their-application-for-solar-cells

[11] Yi, Z. et al. An orthophosphate semiconductor with properties under visible-light irradiation. *Nature Materials*. 9, 559-564 (2010).

[12] Xu, C., Shin, P., Cao, L. & Gao, D. Preferential Growth of Long ZnO Nanowire Array and Its Application in Dye-Sensitized Solar Cells. *J. Phys. Chem. C.* 114, 125-129 (2010).

[13] Wang, M., Wang, Y. & Li, J. ZnO nanowire arrays coating on TiO2 nanoparticles as a composite photoanode for high efficiency DSSC. Chem. Commun. 47, 11246-11248 (2011).

[14] Xu, C., Wu, J., Desai, U.V. & Gao, D. High-Efficiency Solid-State Dye-Synthesized Solar Cells Based on TiO_2-Coated ZnO Nanowire Arrays. *Nano Lett*. 12, 2420-2424 (2012).

[15] Nie, L., Huang, Z. & Zhang, W. Synthesis of Visible-light-driven Photocatalyst Ag_3PO_4 by a Precipitation-replacement Method. *Advanced Materials Research.* 382, 435-438 (2012).

[16] Deng, J., Pang, H., Deng, D. & Zhang, J. Facile control synthesis of Ag_3PO_4 and morphologies effects on their photocatalytic properties. *J Nanoengineering and Nanosystems*. 1-3 (2012).

[17] Khan, A., Qamar, M., & Muneer, M. Synthesis of highly active visible-light-driven colloidal silver orthophosphate. *Chemical Physics Letters*. 519–520, 54–58 (2012).

[18] Umezawa, N., Shuxin, O. & Ye, J. Theoretical study of high photocatalytic performance of Ag_3PO_4. Physical Review. 83, 035202-1 (2011).

[19] Bi, Y., Ouyang, S., Cao, J. & Ye, J. Facile synthesis of rhombic dodecahedral AgX/Ag_3PO_4 (X = Cl, Br, I) heterocrystals with enhanced photocatalytic properties and stabilities. *Phys. Chem. Chem. Phys.* 13, 10071–10075 (2011).

[20] Bi, Y., Ouyang, S., Umezawa, N., Cao, J. & Ye, J. Facet Effect of Single-Crystalline Ag_3PO_4 Sub-microcrystals on Photocatalytic Properties. *J. Am. Chem. Soc.* 133, 6490-6492 (2011).

[21] Dinh, C. T. et al. Large-scale synthesis of uniform silver orthophosphate colloidal nanocrystals exhibiting high visible light photocatalytic activity. *Chem. Commun*. 47, 7797–7799 (2011).

[22] Yao, W. et al. Synthesis and characterization of high efficiency and stable Ag_3PO_4/TiO_2 visible light photocatalyst for the degradation of methylene blue and rhodamine B solutions. *J. Mater. Chem*. 22, 4050-4055 (2012).

[23] Jang, K. et al. Shape-Controlled Synthesis of Silver Sulfide Nanocrystals by Understanding the Origin of Mixed-Shape Evolution. *Chem. Commun. 43,* 4474-4476 (2007).

[24] Ledwith, D., Pillai, S.C., Watson, G.W. & Kelly, J.M. Microwave induced preparation of a-axis oriented double-ended needle-shaped ZnO microparticles. *Chem. Commun*. 20, 2294-2295 (2004)

[25] Negahdary, M., Zarchi, S.R., Rousta, N. & Pour, S.S. Direct Electron Transfer of Cytochrome c on ZnO Nanoparticles Modified Carbon Paste Electrode. *ISRN Biophysics*. 2012, 1-6 (2012).

[26] Ahsanulhaq, Q., Kim, J.H., Kim, J.H. & Hahn, YB. Seedless Pattern Growth of Quasi-Aligned ZnO Nanorod Arrays on Cover Glass Substrates in Solution. *Nano Res Lett*. 5, 669-674 (2010).

[27] Liang, Q., Ma, W., Shi, Y., Li, Z. & Yang, X. Hierarchical Ag_3PO_4 porous microcubes with enhanced photocatalytic properties synthesized with the assistance of trisodium citrate. *CrystEngComm.* (2012).

[28] Tennakone, K., Jayatissa, A.H. & Wijeratne, W. Photocleavage of Water with Silver Phosphate. *J. Chem. Soc., Chem Commun*. 496-498 (1988).

[29] Bi et al. Photocatalytic and photoelectric properties of cubic Ag_3PO_4 sub-microcrystals with sharp corners and edges. *Chem Commun*. 48, 3748-3750 (2012).

[30] Hashimoto, K., Irie, H. & Fujishima, A. TiO_2 Photocatalysis: Historical Overview and Future Prospects. AAPPS Bulletin. 17. 12-28 (2007).

[31] Pokaipisit, A., Horprathum, M., & Limsuwan, P. Influence of Annealing Temperature on the Properties of ITO Films Prepared by Electron Beam Evaporation and Ion-Assisted Deposition. *Kasetsart J. (Nat. Sci.)*. 42, 362-366 (2008).

[32] Mishra, R.L., Mishra, S.K. & Prakash, S.G. Optical and Gas Characteristics of Tin Oxide Nano-Crystalline Thin Film. *Journal of Ovonic Research*. 5, 77-85 (2009).